

## Strong Coupling between Mechanical Modes in a Nanotube Resonator

A. Eichler,<sup>1</sup> M. del Álamo Ruiz,<sup>1</sup> J. A. Plaza,<sup>2</sup> and A. Bachtold<sup>1</sup>

<sup>1</sup>*Institut Català de Nanotecnologia, Campus de la UAB, E-08193 Bellaterra, Spain*

<sup>2</sup>*IMB-CNM (CSIC), E-08193 Bellaterra, Barcelona, Spain*

(Received 17 May 2012; published 11 July 2012)

We report on the nonlinear coupling between the mechanical modes of a nanotube resonator. The coupling is revealed in a pump-probe experiment where a mode driven by a pump force is shown to modify the motion of a second mode measured with a probe force. In a second series of experiments, we actuate the resonator with only one oscillating force. Mechanical resonances feature exotic line shapes with reproducible dips, peaks, and jumps when the measured mode is commensurate with another mode with a frequency ratio of either 2 or 3. Conventional line shapes are recovered by detuning the frequency ratio using the voltage on a nearby gate electrode. The exotic line shapes are attributed to strong coupling between the mechanical modes. The possibility to control the strength of the coupling with the gate voltage holds promise for various experiments, such as quantum manipulation, mechanical signal processing, and the study of the quantum-to-classical transition.

DOI: [10.1103/PhysRevLett.109.025503](https://doi.org/10.1103/PhysRevLett.109.025503)

PACS numbers: 62.25.Jk, 81.07.De, 81.07.Oj

The nonlinear nature of mode coupling lies at the origin of a wide variety of phenomena [1–12], including mechanical synchronization, mechanically induced transparency, and vibration localization. In the case that two modes operate at well separated frequencies, the effect of the coupling is usually modest, and the oscillators move essentially in an independent manner. The coupling between two modes is expected to become strong when the ratio between their resonance frequencies is an integer  $n$  [13]. Perturbation theory then predicts that the motion of one oscillator strongly affects the motion of the other oscillator, and vice versa, through nonlinear forces for which the order of the nonlinearity is  $n$ . Moreover, the resonance line shapes are expected to be peculiar [13]. Strong coupling, also called internal resonance, has not been observed in nanomechanical resonators thus far, because the ratio between the resonance frequencies is usually not an integer.

Resonators based on carbon nanotubes [14–16] provide a unique platform to test mechanics at the nanoscale. A nanotube behaves like a semiflexible polymer in the sense that it can bend and stretch to large extents [17]. Consequently, nonlinearities in nanotube resonators are important and result in unusual behaviors [18–20]. In this work, we take advantage of the mechanical flexibility of nanotubes to achieve strong coupling between mechanical modes. Indeed, the static shape of a nanotube can be deformed to a large extent with the voltage applied on a gate electrode. This enables us to tune the resonance frequencies [14,21] in order to make two modes commensurate. In addition, the oscillation is easily driven to large amplitudes [14] so that nonlinear forces, including coupling forces, are sizable.

In this Letter, we study the line shape of mechanical resonances as a function of gate voltage. Line shapes become exotic, featuring reproducible dips, peaks, and

jumps, when the measured mode is commensurate with another mode with a frequency ratio of either 2 or 3. Conventional line shapes are recovered by detuning the frequency ratio with the gate voltage. These results agree with the predictions of strong coupling. The coupling is attributed to motion-induced tension; that is, the oscillation of one mode induces a mechanical tension in the resonator that affects the dynamics of the other mode, and vice versa.

We employ conventional techniques for the fabrication and the measurements of nanotube resonators. Figures 1(a) and 1(b) show that the nanotube is contacted to two electrodes and is suspended over a trench with a gate electrode at the bottom. The nanotube is grown by chemical vapor deposition in the last step of the fabrication process in order to reduce contamination [22] (Supplemental Material, Sec. I [23]). We check with a scanning electron microscope that only one nanotube is suspended over the trench. The mechanical motion is driven and detected by using the two-source and the frequency-modulation (FM) mixing methods. The two-source method [14], which enables a direct measurement of the amplitude of the motion, is used to record resonance line shapes, whereas the FM method [24] is better at detecting small signals, so we employ it to map resonance frequencies as a function of gate voltage  $V_g$  (Supplemental Material, Sec. II [23]). Measurements are performed between 60 and 70 K to avoid Coulomb blockade at low temperature [15,16].

The nanotube resonator already begins to exhibit Duffing nonlinearities at low driving force  $F_d$  [25]. Figures 1(c) and 1(e) show two resonance line shapes at the lowest  $F_d$  for which we obtain a good signal-to-noise ratio. The two resonances correspond to a single mode at different values of  $V_g$ . The quality factors are 230 and 350 in Figs. 1(c) and 1(e), respectively. Upon doubling  $F_d$ , a hysteresis emerges, marking the onset of the nonlinear

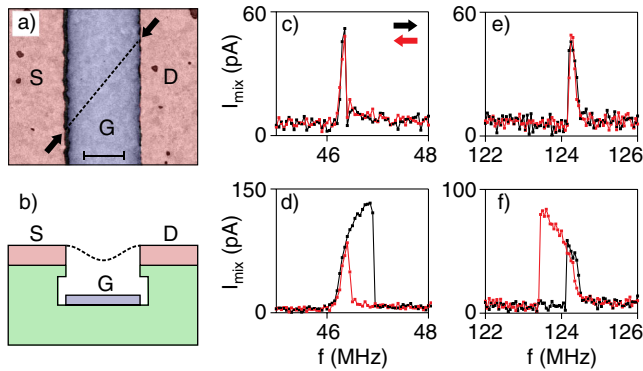


FIG. 1 (color online). Device characterization. (a) Colored scanning electron microscopy image of the device measured in this work with source ( $S$ ), drain ( $D$ ), and gate ( $G$ ) electrodes. The nanotube position is represented by a dashed line, and the clamping points are indicated by arrows. The suspended length of the nanotube is  $1.77 \mu\text{m}$ , and the depth of the trench is  $370 \text{ nm}$ . Scale bar:  $600 \text{ nm}$ . The image is recorded after the measurements of the resonator. (b) Schematic side view of the device. (c)–(f) Mechanical resonances for small and large driving forces obtained by measuring the mixing current ( $I_{\text{mix}}$ ) as a function of the driving frequency ( $f$ ) with the two-source technique. The driving force is electrostatic and is proportional to the oscillating voltage  $V^{ac}$  applied to the gate electrode.  $V^{ac} = 0.2 \text{ mV}$  and  $V_g = 1.5 \text{ V}$  in (c);  $V^{ac} = 0.4 \text{ mV}$  and  $V_g = 1.5 \text{ V}$  in (d);  $V^{ac} = 0.2 \text{ mV}$  and  $V_g = 4 \text{ V}$  in (e);  $V^{ac} = 0.4 \text{ mV}$  and  $V_g = 4 \text{ V}$  in (f). For the detection, we apply an oscillating voltage ( $V_s^{ac} = 0.056 \text{ mV}$ ) to the source electrode. Black (red) curves correspond to upward (downward) sweeps.

regime [Figs. 1(d) and 1(f)]. An estimation of the motional amplitude yields values between 1 and 9 nm in Figs. 1(c)–1(f) (Supplemental Material, Sec. III [23]). Interestingly, the asymmetry of the resonance is different between Figs. 1(d) and 1(f), which indicates different signs of the Duffing force. The sign change occurs around  $V_g = 1.9 \text{ V}$ .

The resonance frequencies can be tuned with  $V_g$  by an amount that is different for each mode [Figs. 2(a) and 2(b)]. The resonance frequency variation is attributed to the mechanical tension that builds up in the nanotube as it bends towards the back gate upon increasing  $V_g$  [14,26]. The amount of the variation depends on the shape and the direction of the mode. Finite element simulations can qualitatively reproduce the measured  $V_g$  dependences of the different resonance frequencies [Fig. 2(c)] without any free parameters using the static shape of the nanotube imaged with a scanning electron microscope (Supplemental Material, Sec. VII [23]). These simulations show that the static deformation of the nanotube towards the gate electrode is as large as  $50 \text{ nm}$  for  $V_g = 4 \text{ V}$  [Fig. 2(d)]. For the simpler case of a straight nanotube, we can describe the  $V_g$  dependences of the resonance frequencies in a satisfactory way using the Euler-Bernoulli equation (Supplemental Material, Sec. VIII [23]); the static deformation is  $17 \text{ nm}$  for  $V_g = 4 \text{ V}$  [Fig. 2(e)].

Coupling between the modes can be observed in a pump-probe experiment [5]. Specifically, we apply a force at frequency  $f_{\text{probe}}$  to probe one mode using the FM

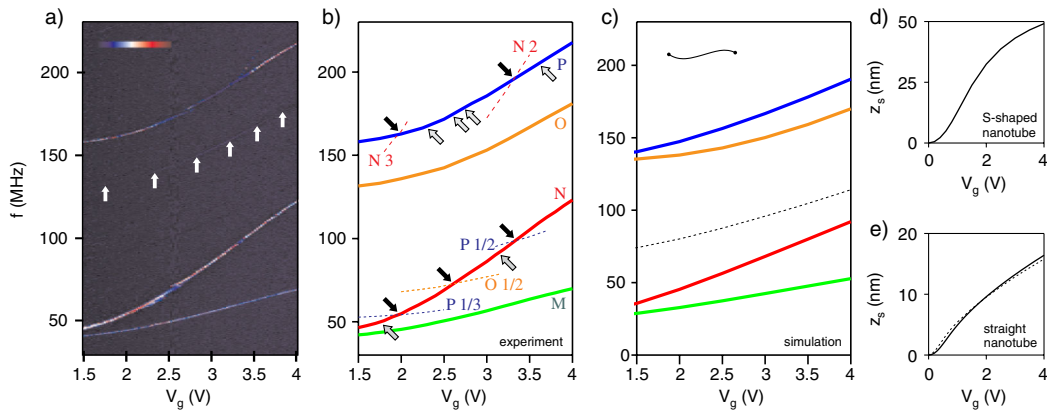


FIG. 2 (color online). Tuning resonance frequencies. (a) Map of resonance frequencies as a function of  $V_g$  (by measuring  $I_{\text{mix}}$  as a function of  $f$  and  $V_g$  for  $V^{ac} = 2 \text{ mV}$  with the FM technique). We clearly discern three modes, while a fourth one is weaker and is indicated by arrows. Color scale: 0 (black) to  $0.1 \text{ nA}$  (red). (b) Schematic of the map of resonance frequencies as a function of  $V_g$ . The four modes are represented by plain lines and labeled  $M$ ,  $N$ ,  $O$ , and  $P$ . Dashed lines correspond to the resonance frequencies of these modes multiplied by 2, 3,  $1/2$ , or  $1/3$  (the values are indicated in the labels). Black arrows point to regions where line shapes are exotic and two modes are commensurate. Gray arrows point to exotic line shape regions for which we cannot assign the coupled mode. (c) Finite element simulation of the map of resonance frequencies as a function of  $V_g$  obtained with ANSYS. The dashed line corresponds to a mode that we have not detected. The simulations show that this mode has one node (while the others have either zero or two nodes) and thus cannot be detected due to symmetry reasons. Inset: Schematic of the static shape of the nanotube when  $V_g = 0 \text{ V}$ . The deformation in the transverse direction is exaggerated with respect to the nanotube length. The largest deformation is  $\sim 40 \text{ nm}$  (Supplemental Material, Sec. VII [23]). (d) Static displacement of the center of the resonator ( $z_s$ ) calculated with ANSYS using the static shape of the nanotube (when  $V_g = 0 \text{ V}$ ) depicted in the inset of (c). (e)  $z_s$  calculated from the Euler-Bernoulli equation for a straight nanotube (plain line). The dashed line corresponds to the result calculated with ANSYS for the same straight nanotube.

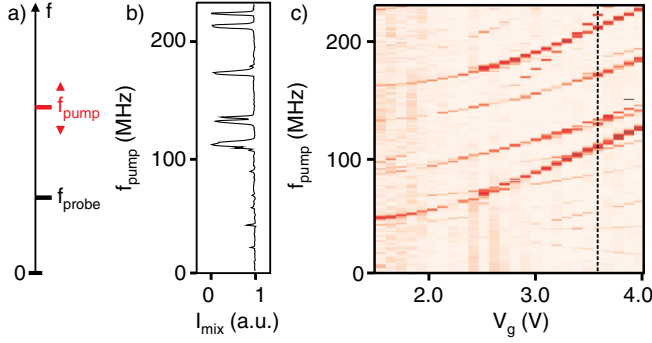


FIG. 3 (color online). Mechanical coupling measured in a pump-probe experiment. (a) Representation of the two drive frequencies used in the pump-probe experiment. The pump force is swept in frequency, whereas  $f_{\text{probe}}$  is set to match the resonance frequency of the lowest mode ( $M$ ). (b) Normalized mixing current of the probed mode as a function of  $f_{\text{pump}}$  at  $V_g = 3.6$  V (measured with the FM technique). Before the scan, we set  $f_{\text{probe}}$  so that the current is maximal ( $I_{\text{mix}}^0$ ). We plot the measured current divided by  $I_{\text{mix}}^0$ . The oscillating voltage of the pump is 5.6 mV, and the FM oscillating voltage of the probe is 2 mV. (c) Normalized mixing current of the probed mode as a function of  $f_{\text{pump}}$  and  $V_g$  using the same parameters as in (b). The line graph in (b) is marked with a dashed line. Color scale:  $I_{\text{mix}} = 0$  (dark red) to  $I_{\text{mix}} = 1$  (white).

method. The current of the probed mode is continuously monitored while sweeping the frequency  $f_{\text{pump}}$  of a second force [Figs. 3(a) and 3(b)]. The sweep in  $f_{\text{pump}}$  is repeated for various values of  $V_g$  [Fig. 3(c)]. The current of the probed mode is found to change when  $f_{\text{pump}}$  matches the resonance frequency (or the harmonic) of another mode [by comparing Fig. 3(c) and Supplemental Material, Fig. S3(a) [23]]. This unambiguously demonstrates that the modes of our nanotube resonator are coupled.

When only one mode is actuated, we observe discontinuities in maps of the resonance frequency as a function of  $V_g$  [Figs. 4(e) and 4(f)]. The discontinuities are accompanied by exotic resonance line shapes [Figs. 4(g)–4(j)]. These features often occur when the resonance frequency of the measured mode is equal to that of another mode multiplied by 2, 3, 1/2, or 1/3 [as indicated by the black arrows in Fig. 2(b) [27]]. Upon detuning the frequency ratio using  $V_g$ , conventional resonance line shapes are recovered [Figs. 4(a) and 4(d)]. Another way to retrieve regular line shapes is to reduce the driving force (Supplemental Material, Sec. XIII [23]). We also observe exotic line shapes [indicated by gray arrows in Fig. 2(b)] without being able to identify the second mode; we speculate that the second mode is not detectable with the mixing technique or that it oscillates in a frequency range that has not been probed.

These experimental findings are consistent with the theory of strong coupling between mechanical modes in a resonator [13,28]. The observation that strong coupling

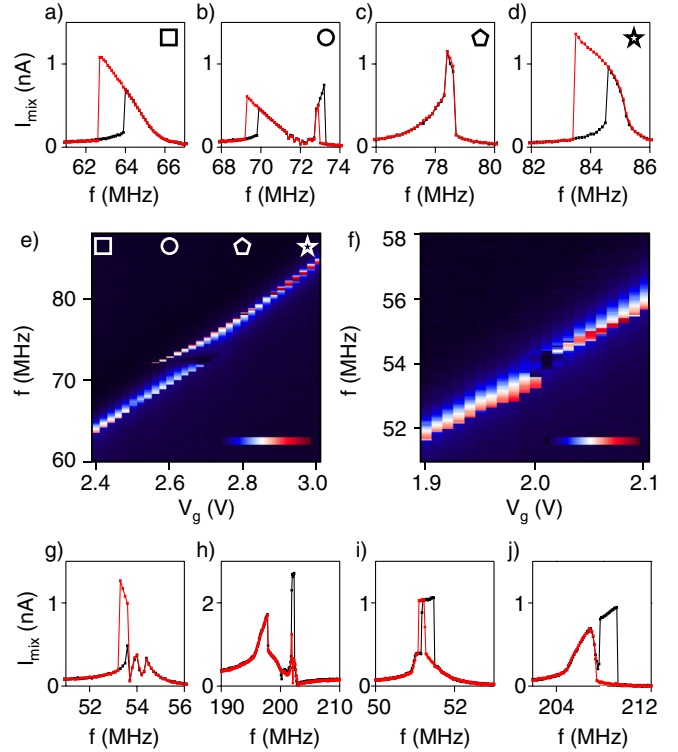


FIG. 4 (color online). Resonances when the measured mode is commensurate or nearly commensurate with another mode. (a)–(d) Resonance line shapes of one mode for different  $V_g$  measured with the two-source technique. The driving voltage applied to the gate electrode is  $V^{ac} = 1.1$  mV, and the voltage applied for the detection on the source electrode is  $V_s^{ac} = 0.56$  mV. Black (red) curves correspond to upward (downward) sweeps.  $V_g = 2.4$  V in (a);  $V_g = 2.6$  V in (b);  $V_g = 2.8$  V in (c);  $V_g = 3$  V in (d). (e) Map of the resonance frequency as a function of  $V_g$  (obtained by measuring  $I_{\text{mix}}$  as a function of  $f$  and  $V_g$  for  $V^{ac} = 1.1$  mV and  $V_s^{ac} = 0.56$  mV using the two-source technique by increasing  $f$ ). Color scale: 0 (black) to 1 nA (red). (f) Map of the resonance frequency as a function of  $V_g$  (obtained for  $V^{ac} = 1.1$  mV and  $V_s^{ac} = 0.28$  mV using the two-source technique by decreasing  $f$ ). Color scale: 0 (black) to 0.7 nA (red). (g)–(j) Resonance line shapes for different modes and different values of  $V_g$  measured with the two-source technique.  $V^{ac} = 1.1$  mV,  $V_s^{ac} = 0.56$  mV, and  $V_g = 1.98$  V in (g).  $V^{ac} = 17$  mV,  $V_s^{ac} = 1.1$  mV, and  $V_g = 3.41$  V in (h).  $V^{ac} = 1.7$  mV,  $V_s^{ac} = 0.28$  mV, and  $V_g = 1.86$  V in (i).  $V^{ac} = 5.6$  mV,  $V_s^{ac} = 0.56$  mV, and  $V_g = 3.6$  V in (j).

occurs for a frequency ratio of 2 or 3 implies that quadratic and cubic nonlinear forces are important and that the equation of motion for mode  $i$  is of the form

$$\frac{d^2 z_i}{dt^2} = -\omega_i^2 z_i - \gamma \frac{dz_i}{dt} - \alpha_2 z_i^2 - \alpha_3 z_i^3 - \sum_{j,k} \beta_{jk} z_j z_k - \sum_{j,k,l} \epsilon_{jkl} z_j z_k z_l + g \quad (1)$$

with  $z_i$  the motional amplitude,  $t$  the time,  $\omega_i$  the angular resonance frequency, and  $g$  the effective force normalized

by the mass [13];  $\gamma$ ,  $\alpha_2$ ,  $\alpha_3$ ,  $\beta_{jk}$ , and  $\epsilon_{jkl}$  are various constants. We omit the nonlinear damping force for simplicity [18]. Mode  $i$  couples to modes  $j$ ,  $k$ , and  $l$  through the forces  $z_j z_k$  and  $z_j z_k z_l$  (Supplemental Material, Sec. IX [23]).

Quadratic and cubic nonlinear forces ( $z_i^2$ ,  $z_i^3$ ,  $z_j z_k$ , and  $z_j z_k z_l$ ) naturally emerge from the tension in the beam that is induced by motion—the beam is stretched and compressed periodically in time, because it is clamped at both ends. The  $z_i^2$  and  $z_i^3$  forces are responsible for the hystereses and the asymmetric resonance line shapes in Figs. 1(d) and 1(f). The upward asymmetry in Fig. 1(d) is associated with the cubic  $z_i^3$  force, since motion-induced tension leads to a positive coefficient  $\alpha_3$ . When the static deformation of the beam  $z_s$  becomes sizable, the quadratic  $z_i^2$  force can lead to a reversal of the asymmetry [29,30]. We estimate from the asymmetries in Figs. 1(d) and 1(f) that  $z_s$  is 2.8 and 13 nm at  $V_g = 1.5$  and 4 V, respectively (Supplemental Material, Sec. XI [23]). This is in fair agreement with the calculation in Fig. 2(e), which supports that the nonlinear  $z_i^2$  and  $z_i^3$  forces originate from motion-induced tension. We estimate that these forces are 3 orders of magnitude larger than electrostatic nonlinear forces [29] and thus neglect the latter (Supplemental Material, Sec. XII [23]). The coupling forces  $z_j z_k$  and  $z_j z_k z_l$  are intimately related to the  $z_i^2$  and  $z_i^3$  forces, since they all arise in the same way from the Euler-Bernoulli equation (Supplemental Material, Sec. IX [23]). It is thus likely that the modal coupling in our experiment is also due to motion-induced tension. In other words, the coupling is mediated by the tension generated by the oscillation of one mode, which affects the dynamics of the other mode, and vice versa. The solutions of the equations of motion that describe motion-induced tension [Eq. (1)] are characterized by exotic line shapes for the case of commensurable resonance frequencies [13]. The line shapes are sensitive to the coefficients of the coupling forces in a critical fashion. A detailed comparison between the experiment and theory is not possible at the moment, since the coefficients depend on the static shape of the nanotube, which is not known precisely enough.

The exotic line shapes in nanotube resonators are analogous to Fermi resonances observed in the infrared and Raman spectra of molecules [31,32]. When the frequency of a vibrational mode of a molecule is twice as large as that of another mode, energy can be transferred from one mode to the other. This leads to a mixing of the eigenfunctions and to unusual spectra. However, the coupling between the vibrational modes cannot be externally tuned as in nanotube resonators.

The mode coupling force can be made larger in nanotube resonators than in resonators made from other materials, since the coupling force scales inversely with the fourth power of the resonator length (Supplemental Material, Sec. IX [23]) and nanotube resonators can be as short as

$\sim 100$  nm [33,34]. Mode coupling is further enhanced by the excellent material characteristics of nanotubes, since the coupling force is linearly proportional to  $E/\rho$  (Supplemental Material, Sec. IX [23]) and nanotubes have a high Young modulus  $E$  and a low mass density  $\rho$ .

The achievement of strong coupling combined with the possibility to tune its strength opens up many possibilities. Such coupling may lead to sizable signatures in the quantum-to-classical transition of a mechanical resonator [35]. In the quantum regime, it may allow for the manipulation of energy quanta between different mechanical modes using gate voltage pulses. Classically, the transfer of energy between mechanical modes could be made faster than the energy relaxation time, which is interesting for high-speed signal operation [11,36–38]. The nonlinear nature of strong coupling is expected to give rise to non-intuitive behaviors that have not been tested thus far [13]. A striking example is that driving one of two coupled modes can cause the second mode to reach a higher amplitude than that of the driven one.

When finalizing this Letter, we became aware of the paper by Antonio, Zanette, and López [39] that reports on strong coupling in a 0.5 mm long micromechanical resonator. The frequency of the modes is tuned by increasing the driving force (through the Duffing force). The possibility to tune the resonance frequencies of a nanotube resonator with a gate voltage is more convenient for practical use.

We thank M. Dykman, A. Isacsson, E. Weig, and H. Yamaguchi for discussions. We acknowledge support from the European Union through the RODIN-FP7 project, the ERC-carbonNEMS project, and a Marie Curie grant (No. 271938), the Spanish ministry (FIS2009-11284), and the Catalan government (AGAUR, SGR). The ANSYS simulation software was financially supported by the MINAHE3 and MINAHE4 projects (Ref. TEC2008-06883-C03-01 and TEC2011-29140-C03-01). We thank Brian Thibeault (Santa Barbara) for help in fabrication.

- 
- [1] M. Sato, B.E. Hubbard, A.J. Sievers, B. Ilic, D.A. Czaplewski, and H.G. Craighead, *Phys. Rev. Lett.* **90**, 044102 (2003).
  - [2] M.C. Cross, A. Zumdieck, R. Lifshitz, and J.L. Rogers, *Phys. Rev. Lett.* **93**, 224101 (2004).
  - [3] E. Gil-Santos, D. Ramos, A. Jana, M. Calleja, A. Raman, and J. Tamayo, *Nano Lett.* **9**, 4122 (2009).
  - [4] R.B. Karabalin, M.C. Cross, and M.L. Roukes, *Phys. Rev. B* **79**, 165309 (2009).
  - [5] H.J.R. Westra, M. Poot, H.S.J. van der Zant, and W.J. Venstra, *Phys. Rev. Lett.* **105**, 117205 (2010).
  - [6] I. Mahboob, Q. Wilmar, K. Nishiguchi, A. Fujiwara, and H. Yamaguchi, *Phys. Rev. B* **84**, 113411 (2011).
  - [7] W.J. Venstra, H.J.R. Westra, and H.S.J. van der Zant, *Appl. Phys. Lett.* **99**, 151904 (2011).

- [8] R. B. Karabalin, R. Lifshitz, M. C. Cross, M. H. Matheny, S. C. Masmanidis, and M. L. Roukes, *Phys. Rev. Lett.* **106**, 094102 (2011).
- [9] T. Faust, J. Rieger, M. J. Seitner, P. Krenn, J. P. Kotthaus, and E. M. Weig, *Phys. Rev. Lett.* (to be published).
- [10] T. Antoni, K. Makles, R. Braive, T. Briant, P.-F. Cohadon, I. Sagnes, I. Robert-Philip, and A. Heidmann, [arXiv:1202.3675v1](https://arxiv.org/abs/1202.3675v1).
- [11] I. Mahboob, K. Nishiguchi, H. Okamoto, and H. Yamaguchi, *Nature Phys.* **8**, 387 (2012).
- [12] K. J. Lulla, R. B. Cousins, A. Venkatesan, M. J. Patton, A. D. Armour, C. J. Mellor, and J. R. Owers-Bradley, [arXiv:1204.4487v1](https://arxiv.org/abs/1204.4487v1).
- [13] A. H. Nayfeh and D. T. Mook, *Nonlinear Oscillations* (Wiley-VCH, New York, 1979).
- [14] V. Sazonova, Y. Yaish, H. Üstünel, D. Roundy, T. A. Arias, and P. L. McEuen, *Nature (London)* **431**, 284 (2004).
- [15] B. Lassagne, Y. Tarakanov, J. Kinaret, D. Garcia-Sanchez, and A. Bachtold, *Science* **325**, 1107 (2009).
- [16] G. A. Steele, A. K. Hüttel, B. Witkamp, M. Poot, H. B. Meerwaldt, L. P. Kouwenhoven, and H. S. J. van der Zant, *Science* **325**, 1103 (2009).
- [17] J.-P. Salvetat, J.-M. Bonard, N. H. Thomson, A. J. Kulik, L. Forró, W. Benoit, and L. Zuppiroli, *Appl. Phys. A* **69**, 255 (1999).
- [18] A. Eichler, J. Moser, J. Chaste, M. Zdrojek, I. Wilson-Rae, and A. Bachtold, *Nature Nanotech.* **6**, 339 (2011).
- [19] J. Atalaya, A. Isacsson, and M. I. Dykman, *Phys. Rev. Lett.* **106**, 227202 (2011).
- [20] A. W. Barnard, V. Sazonova, A. M. van der Zande, and P. L. McEuen, [arXiv:1110.1517v1](https://arxiv.org/abs/1110.1517v1).
- [21] A. Eichler, J. Chaste, J. Moser, and A. Bachtold, *Nano Lett.* **11**, 2699 (2011).
- [22] A. K. Hüttel, G. A. Steele, B. Witkamp, M. Poot, L. P. Kouwenhoven, and H. S. J. van der Zant, *Nano Lett.* **9**, 2547 (2009).
- [23] See Supplemental Material at <http://link.aps.org/supplemental/10.1103/PhysRevLett.109.025503> for further discussions on fabrication, measurement details, and experiment analysis.
- [24] V. Gouttenoire, T. Barois, S. Perisanu, J.-L. Leclercq, S. T. Purcell, P. Vincent, and A. Ayari, *Small* **6**, 1060 (2010).
- [25] H. W. Ch. Postma, I. Kozinsky, A. Husain, and M. L. Roukes, *Appl. Phys. Lett.* **86**, 223105 (2005).
- [26] C. Chen, S. Rosenblatt, K. I. Bolotin, W. Kalb, P. Kim, I. Kymissis, H. L. Stormer, T. F. Heinz, and J. Hone, *Nature Nanotech.* **4**, 861 (2009).
- [27] We do not observe exotic line shapes for modes  $M$  and  $O$ , probably because these modes are difficult to actuate with the gate electrode [Supplemental Material, Fig. S2(a) [23]] and that the motional amplitude remains low even for large values of  $V^{ac}$ . Modes  $M$  and  $O$  move essentially parallel to the gate electrode (Supplemental Material, Sec. IV [23]).
- [28] In the pump-probe experiment in Fig. 3, we drive both the pumped and the probed modes. The motion of the pumped mode modifies the dynamics of the probed mode, such as its resonance frequency, through nonlinear coupling forces [5]. In Fig. 4, the coupling can be revealed by driving only one of the two modes. Indeed, when the frequency ratio between two modes is an integer, energy can easily be transferred from one mode to the other through nonlinear forces so that driving one mode induces the motion of the other. The situation becomes then similar to that of the pump-probe experiment in the sense that two modes are oscillating.
- [29] I. Kozinsky, H. W. Ch. Postma, I. Bargatin, and M. L. Roukes, *Appl. Phys. Lett.* **88**, 253101 (2006).
- [30] M. I. Dykman and M. A. Krivoglaz, *Phys. Status Solidi B* **48**, 497 (1971).
- [31] E. Fermi, *Z. Phys.* **71**, 250 (1931).
- [32] G. Herzberg, *Molecular Spectra and Molecular Structure*, Vol. II (Van Nostrand, Princeton, 1956).
- [33] J. Chaste, M. Sledzinska, M. Zdrojek, J. Moser, and A. Bachtold, *Appl. Phys. Lett.* **99**, 213502 (2011).
- [34] E. A. Laird, F. Pei, W. Tang, G. A. Steele, and L. P. Kouwenhoven, *Nano Lett.* **12**, 193 (2012).
- [35] I. Katz, A. Retzker, R. Straub, and R. Lifshitz, *Phys. Rev. Lett.* **99**, 040404 (2007).
- [36] N. Liu, F. Giesen, M. Belov, J. Losby, J. Moroz, A. E. Fraser, G. McKinnon, T. J. Clement, V. Sauer, W. K. Hiebert, and M. R. Freeman, *Nature Nanotech.* **3**, 715 (2008).
- [37] Q. P. Unterreithmeier, T. Faust, and J. P. Kotthaus, *Phys. Rev. B* **81**, 241405(R) (2010).
- [38] H. Yamaguchi, H. Okamoto, and I. Mahboob, *Appl. Phys. Express* **5**, 014001 (2012).
- [39] D. Antonio, D. H. Zanette, and D. López, *Nature Commun.* **3**, 806 (2012).